

In-Situ Mechanical Testing for Characterizing Strain Localization During Deformation at Elevated Temperatures

J.L. Walley · R. Wheeler · M.D. Uchic · M.J. Mills

Received: 19 November 2010 / Accepted: 7 April 2011 / Published online: 14 May 2011
© Society for Experimental Mechanics 2011

Abstract An experimental methodology has been developed to characterize local strain heterogeneities in alloys via *in-situ* scanning electron microscope (SEM) based mechanical testing. Quantitative measurements of local strains as a function of grain orientation, morphology and neighborhood are crucial for mechanistic understanding and validation of crystal plasticity models. This study focuses on the technical challenges associated with performing creep tests at elevated temperatures $\leq 700^\circ\text{C}$ in an SEM. Samples of nickel-based superalloy Rene 104 were used for this study, but the technique is applicable to testing of any metal samples at elevated temperature. Electron beam lithography was employed to produce a suitable surface speckle pattern of hafnium oxide to facilitate full field displacement measurements using a commercial software package. The speckle pattern proved to have good thermal stability and provided excellent contrast for image acquisition using secondary

electron imaging at elevated temperature. The speckle pattern and microscope magnification were optimized to obtain the resolution necessary to discern strain localizations within grain interiors and along grain boundaries. Minimum strain resolution due to SEM image distortions was determined prior to tensile testing, and image integration methods were utilized to minimize imaging artifacts. Limitations due to the present specimen heating method and potential solutions to these limitations are also addressed.

Keywords Elevated temperature tension experiment · Scanning electron microscopy · 2D digital image correlation · Speckle pattern development · Nickel-based superalloy

Introduction

One of the issues limiting the development of physics-based deformation models of polycrystalline materials is the lack of experimental validation data that characterizes local strain variations at the grain size scale for relevant usage temperatures and loading conditions. Tests on single crystal samples can provide detailed information on the ‘single grain’ mechanical behavior as a function of crystallographic orientation, but these methods often require specialized sample preparation techniques and do not provide direct information about the processes that allow for strain transmission across grain boundaries [1, 2]. Traditional tensile and creep tests on polycrystalline materials characterize average properties but provide limited insight into local deformation behavior. Empirical evidence describing the temporal development of local plastic flow is greatly desired. Therefore, novel experimen-

J.L. Walley (✉) · M.J. Mills
The Ohio State University,
477 Watts Hall, 2041 College Rd.,
Columbus, OH 43210, USA
e-mail: walley.7@osu.edu

M.J. Mills
e-mail: mills.108@osu.edu

R. Wheeler
UES, Inc.,
4401 North Dayton-Xenia Rd.,
Dayton, OH 45432, USA
e-mail: Robert.Wheeler@wpafb.af.mil

M.D. Uchic
Air Force Research Laboratory, Materials & Manufacturing
Directorate, AFRL/RXLM, Wright Patterson AFB,
Dayton, OH 45433, USA
e-mail: Michael.Uchic@wpafb.af.mil



tal techniques are being developed to characterize the grain and sub-grain scale deformation fields produced during deformation of polycrystalline materials.

Digital image correlation (DIC) methods that utilize optical imaging are readily available for measuring macro-scale planar 2-D, and arbitrary 3-D, motion and deformation [3]. DIC methods were proposed and developed in the early 80's, and have since become widely accepted methods of measuring surface displacements [3]. DIC uses a set of algorithms to correlate local displacements of a sample surface between a reference image and subsequent images that are collected during sample deformation [3, 4]. Correlation occurs by dividing images into subsets and applying a displacement vector to the deformed subset to minimize a normalized cross-correlation criterion (normalized sum of differences is an example) between the deformed subset and the reference subset. Minimizing a normalized cross-correlation criterion allows for correct correspondence between images with slight variations in gray-scale intensity values, i.e. changes in optical lighting or inadequate dissipation of electrons in scanning electron microscopy (SEM) imaging. Often a speckle pattern is generated on the sample surface to provide a unique random pattern to optimize subset correlation. Optical imaging techniques are applicable for characterizing sub-grain deformation heterogeneities in single crystal materials and materials with very large grain sizes [5]. However, optical imaging methods can not provide the needed resolution to discern local displacements in fine grained materials such as nickel-based superalloys. SEM imaging has superior resolution as compared to optical microscopy, and techniques have been developed to use SEM to characterize strain heterogeneities on the 50–1000 μm grain size scale [4, 6–10]. Work by Sutton and coworkers have examined many issues related to *in-situ* SEM-based DIC analysis using a random speckle pattern [7, 8]. Their studies have shown that several SEM image distortions must be taken into consideration when evaluating small amounts of strain accumulation, particularly signal noise and random linear distortions due to beam rastering. Others have utilized a regular repeating grid pattern to characterize both room temperature deformation, by *in-situ* imaging [6], and elevated temperature deformation, by *ex-situ* imaging [4, 9, 10]. Collectively, these studies have shown that the primary limitations for developing an *in-situ* SEM-based elevated temperature strain mapping technique include developing a stable speckle pattern that is of sufficient detail to achieve the desired resolution while the sample is at temperature, developing techniques to maintain specimen thermal stability, and limiting creep of the specimen while the images are being acquired.

This paper highlights the development of an *in-situ*, elevated-temperature tensile technique that operates in-

side of an SEM to characterize the local deformation behavior in wrought nickel-based superalloys. Although the methodology has been optimized for this one material class, it is generally applicable to testing a variety of materials at elevated temperature. This work builds on the room temperature experiments conducted by Sutton, while exploring the added complexities of conducting *in-situ* work at elevated temperature. The methodology described herein includes a protocol for characterizing the grain microstructure of samples prior to testing and correlating these features to the DIC measurements, the development of a high-resolution speckle patterning technique suitable for elevated temperature DIC measurements, identification and mitigation of issues related to both image acquisition and stable uniform heating of the sample during testing, and demonstration of the method via creep at 700°C.

Experimental Procedures

Material

The material examined in this study is γ' -strengthened nickel-base superalloy Rene 104 (15wt% Cr, 18.2% Co, 3.8% Mo, 1.9% W, 1.4% Nb, 3.5% Al, 3.5% Ti, 2.7% Ta, 0.03% C, 0.03% B, 0.05% Zr, balance Ni) [11]. The material was heat treated above the γ' solvus temperature and aged to produce a microstructure consisting of relatively planar grain boundaries with an average grain size of $32\pm 4\ \mu\text{m}$ and a bimodal γ' distribution.

Sample Preparation

Flat dog-bone samples were prepared from the bulk using electrical discharge machining. The dimensions of the gage section of the sample were as follows: a gage length of 1.78 cm, and a rectangular cross-section nominally $0.31\ \text{cm} \times 0.081\ \text{cm}$. Prior to elevated temperature testing, samples were prepared for SEM imaging using conventional polishing techniques on an Allied Multiprep system, culminating with a final vibratory polish using $0.02\ \mu\text{m}$ colloidal silica. After polishing, four microhardness indents were placed near the center of the gage section to define the four corners of a $0.01\ \text{cm}^2$ square. These hardness indents were used to define the location where the speckle pattern was subsequently deposited on the surface, and were also useful in coarse registration of microstructural images and electron backscatter diffraction (EBSD) data with the local displacement maps. Next, the samples were characterized via EBSD mapping and a speckle pattern was deposited using parameters described below. Once patterned, two

type K thermocouples were spot welded onto the surface along the gage length on opposite sides of the patterned area, as shown in Fig. 1.

Characterization Techniques

Electron backscatter diffraction (EBSD) mapping was used to characterize both the grain size and grain orientation with respect to the tensile axis. Mapping was conducted on an FEI ESEM XL-30 SEM outfitted with an EDAX TSL orientation image mapping system. Grains were defined as regions containing at least 5 contiguous data points, with less than 5° misorientation between adjacent data points. Twin boundaries of $\Sigma 3$ orientation were not included in grain size calculations.

Speckle Patterning

Correlated Solutions Inc. VIC-2D digital image correlation software was used to analyze local deformation fields. The DIC software produces optimum accuracy when the minimum speckle size is at least three pixels, and a greater number of speckles per grain produces a more detailed characterization of the strain distribution within each grain [3, 12]. With an average grain size of $32 \pm 4 \mu\text{m}$, it was desired to make the subset size less than half the average linear grain size, $\sim 10 \mu\text{m}$. Image resolution was set at 2048×1768 . For an image to incorporate 15 grains across the longest dimension the image, a resolution of $6.8 \text{ pixel}/\mu\text{m}$ is required. Based on these resolution requirements and the minimum speckle size criteria mentioned above, a random pattern was generated using square speckles with a size range between 0.45 and $0.7 \mu\text{m}$. In addition to the random speckle pattern, a regular repeating grid with node spacing of $10 \mu\text{m}$ was added to allow for traditional grain boundary sliding

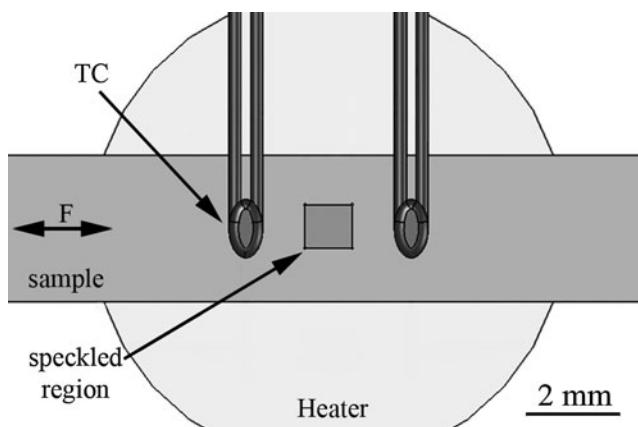


Fig. 1 Schematic diagram showing the locations of the speckled area, two type K thermocouples located on the sample surface, and the size and placement of the resistance specimen heater with respect to the sample. The loading direction (F) is along the horizontal axis

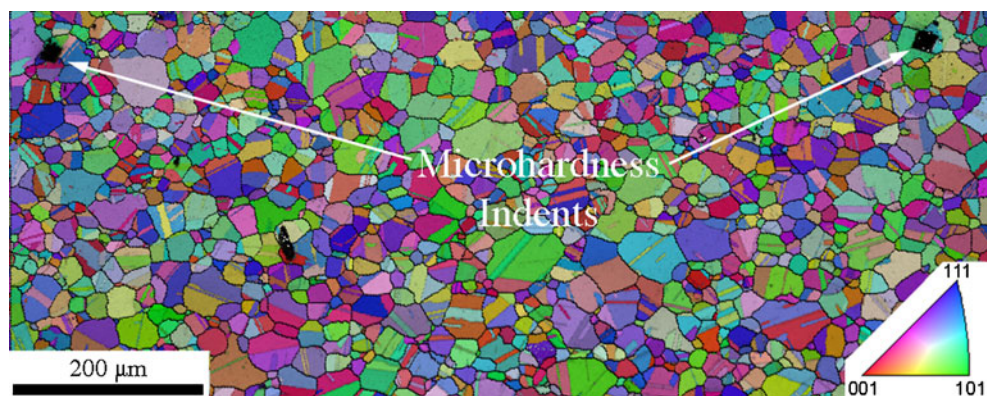
measurements [13]. The pattern also incorporated a set of alpha-numeric markers every $200 \mu\text{m}$ in order to help facilitate locating particular regions within the 0.01 cm^2 analysis area after testing. Electron beam (e-beam) lithography was used to fabricate the desired pattern. This technique uses a focused scanning e-beam to locally expose photo-resist on the sample surface, which results in a highly repeatable point-by-point constructed pattern [14]. Once exposed, the resist is developed to remove the exposed resist and metal or dielectric is deposited onto the sample surface. After deposition the developed resist is removed to reveal the pattern. Following standard clean room procedures, 950 k A4 PMMA resist was spin coated onto the sample surface. Once coated, the sample was exposed at 50 keV with an $800 \text{ uC}/\text{cm}^2$ dose using a Vistec EBPG 5000 e-beam lithography system. The resist was developed in a 1:3 mixture of methyl isobutyl ketone and isopropyl alcohol. As previously mentioned, the location of the speckle pattern on the sample surface was determined by the microhardness indents placed on the surface before EBSD analysis, as shown in Fig. 2. A Denton 502A evaporator was utilized to deposit a 100 nm thick layer of hafnium oxide onto the surface. Once coated, the developed resist was lifted off the sample using an acetone bath, leaving the oxide speckles on the sample surface. A secondary electron image of the speckle pattern is shown in Fig. 3.

Experimental Test Set-Up

An Ernest Fullam® tensile stage was used to perform the *in-situ* mechanical test. The stage can apply loads up to 4448 N and provide measurements of both load and crosshead displacement. The data acquisition system provided with the test frame was used to acquire load and displacement data every second. A molybdenum resistance heater capable of heating to temperatures up to 1200°C was used to heat the sample. The resistance heater is fastened to the tensile frame using six alignment screws, and these screws allow the heater to be carefully positioned in direct contact with the backside of the specimen surface without imparting significant out-of-plane loads.

In order to characterize the performance of the test frame at elevated temperatures, a sample was subjected to various thermal cycles to determine limitations of both the imaging system and the tensile stage. Elevated temperature image acquisition capabilities of the SEM were assessed by imaging a specimen, which was incrementally heated to 700°C at 100°C intervals. At each interval, the sample was held at temperature for 3–5 min before backscatter (BSE) and secondary (SE) electron images were acquired. This same sample was also subjected to loading and unloading at different rates from 0.01 – 0.003 mm/s (5.6×10^{-4} – $1.7 \times$

Fig. 2 Inverse pole figure map of the Rene 104 microstructure showing the location of the microhardness indents that define the speckle pattern region. Colors represent grain orientation normal to the sample surface as defined by the stereographic triangle inset in the lower right corner of the image



10^{-4} s^{-1}) to determine the effect of strain rate on the thermal stability of the sample.

Elevated temperature testing was conducted in a stepwise fashion in an attempt to minimize creep while imaging. The sample was loaded in displacement control, at 0.003 mm/s, to 337 MPa and subsequently held in load control while a pair of images were acquired. These images were used as the reference images for strain analysis. The sample was further loaded in displacement control, at the same rate, to 1100 MPa and held in load control for 35 min to allow for creep deformation. Note that no images were acquired during creep loading. After the prescribed period of time, the sample was unloaded in displacement control to 80% of peak load, and held for 5 min. During this second hold, secondary electron images were acquired for DIC analysis. The sample was reloaded to 1100 MPa and the sequence was repeated for the duration of the experiment.

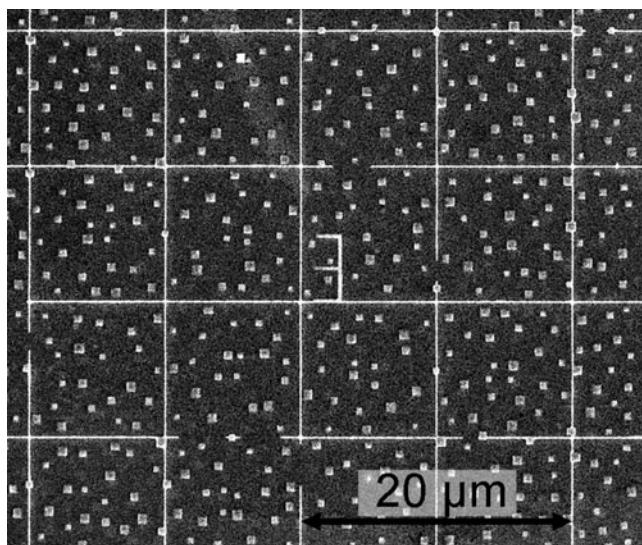


Fig. 3 SEM secondary electron image of the hafnium oxide speckle pattern created by e-beam lithography. Also shown is the grid pattern for grain boundary sliding measurements and an alpha-numeric marker

SEM operating parameters were as follows: 15 kV accelerating voltage, image size of 2048×1768 pixels, and one of two imaging conditions: (a) a single scan at 8 microsecond pixel dwell time, or (b) a pixel dwell time of 1 microsecond, integrating eight frames. Both imaging conditions correspond to a total image acquisition time of 32 seconds. Images were taken at $1000\times$ magnification corresponding to an approximate pixel size of 150 nm.

Correlated Solutions VIC-2D software was selected for conducting digital image correlation to determine local displacement and strain distributions. Analysis was conducted using 60×60 pixel ($9 \times 9 \mu\text{m}$) subset size, and a spacing between subset centers of 3 pixels. No distortion corrections were conducted for strain analysis. Lagrangian strains were calculated using the VIC-2D post processing tab, using a 15 size decay filter. The subset size and spacing can have a dramatic effect on the magnitude and distribution of the calculated strain data; these effects were not addressed in this paper, but should be optimized for the particular imaging set-up.

Results

Microstructural Characterization

Distortions in the EBSD images did not allow for direct overlay of the data with BSE and SE images taken prior creep testing. The use of a commercial SEM calibration standard showed that the lack of one-to-one correlation between the BSE/SE images and EBSD maps was caused by distortions in the EBSD data. For qualitative purposes, distortions in EBSD maps were corrected with image processing software. First, the centers for the hardness indents were used for a rough correlation, and then particular grain boundaries with high BSE contrast were used to further match EBSD data with BSE images to within pixel resolution. This qualitative alignment allows

for direct overlay of the displacement and strain measurements with the EBSD maps.

Speckle Pattern

For both BSE and SE images, the hafnium oxide speckles appear bright as compared to the nickel surface, as shown in the secondary electron image in Fig. 3. Therefore, care was taken during image acquisition to optimize image brightness and contrast to insure that the grey level distribution was not saturated due to the presence of very bright speckles on the dark background. This improved the quality of the image correlation as the VIC-2D correlation works best when the speckle pattern produces a random grayscale pattern at the subset scale. For this work, the subset area was on the order of $81 \mu\text{m}^2$, which encompasses several speckles in each subset.

Experimental Limitations

High temperature imaging

In order to determine the best imaging conditions for high temperature DIC testing, a series of incremental heating experiments were performed at 100°C intervals up to a maximum temperature of 750°C . One of the findings from these experiments was that BSE imaging was only possible to about 300°C , above which thermal radiation significantly degraded the image; this observation is consistent with other studies [15, 16]. By comparison, secondary electron images showed only minimal degradation in quality up to 750°C . For prolonged exposure to temperatures at and above 700°C , white lines appeared in the SE images that degraded the quality of the image. These imaging artifacts were removed by placing an aluminum foil heat shield between the SE detector and the specimen heater. This heat shield limited radiative heat transfer to the secondary electron detector, enabling the use of the secondary electron imaging for these elevated temperature experiments.

Images during creep testing were acquired at regular time intervals. The load was reduced to 80% of the testing condition (880 MPa for 1100 MPa testing condition). These unloading intervals were dependent on the expected creep rate as extrapolated from traditional testing, i.e. shorter intervals for faster creep rates and longer intervals for slower creep rates. Intervals were determined based on the desire for enough strain accumulation to occur that each interval provided unique strain data. A valuable time interval was determined by estimating the required length of time needed such that the average strain would increase by more than three times the noise limits. For this experiment, a 20% drop in applied load arrested creep deformation during imaging, for slow strain rate experi-

ments this unloading might not be necessary and for higher strain rates the unloading during imaging would need to be more dramatic and should be determined for each material type. Assuming uniform deformation, the maximum creep rate above which a stress drop would be required can be calculated as a function of imaging parameters and noise in the calculated strain data, discussed below. For this experimental set-up that would be approximately $4 \times 10^{-5} \text{s}^{-1}$, but since deformation is not uniform and can vary dramatically it would be expected that this is not a conservative estimate.

Specimen thermal stability

During the initial assessment of the test frame performance, loading and unloading of a sample with two welded thermocouples showed that displacement rates of 0.01 and 0.005 mm/s produced substantial and repeatable fluctuations in the sample temperature. The source of these fluctuations is tentatively linked to changes in the total contact surface area of the backside of the specimen and the resistance heater during testing. When the displacement rate was reduced to 0.003 mm/s, these thermal fluctuations were eliminated, presumably because the response time for the thermal controller and substrate heater is commensurate with the variation in contact that may occur during the test at lower strain rate. Since a goal of the present investigation is to study time-dependent deformation processes, testing at slower strain rates is not a severe limitation.

The two thermocouples on the sample surface allowed for the measurement of a possible thermal gradient along the gage length due to improper alignment of the resistance heater and the specimen surface. The temperature acquisition equipment was calibrated to within $\pm 2^\circ\text{C}$. Therefore, the two thermocouples on the sample surface should read the same value, within $\pm 4^\circ\text{C}$, if the specimen heater is properly aligned relative to the sample surface. A sample was heated to 700°C prior to tensile testing to validate that the heater was evenly contacting the specimen surface. In an iterative fashion, the specimen heater was tilted until the two thermocouples read within 7°C of each other.

In-Situ Strain Mapping

VIC-2D calibration and distortion corrections

As previously mentioned in the introduction, the study by Sutton and coworkers showed that SEM images contain several linear distortions that can limit the resolution of image correlation displacement measurements [7, 8]. A conclusion from that study was that conducting integrated image scans eliminates the linear distortions seen when

correlating single scan images taken at $5000\times$ magnification, while at $200\times$ magnification these linear distortions were not observed. In an effort to characterize the performance of the SEM used in our study, at the particular magnification of interest ($1000\times$), pairs of images of the same region of the sample were first acquired at room temperature with zero load without moving the sample using both a single scan with an 8 microsecond dwell time and an eight image integrated scan at 1 microsecond dwell time. Analysis of these images using VIC-2D DIC provides a base-line estimation of the image distortions caused by the SEM optics. It can be seen in Fig. 4(a) and (b) that no linear distortions in the displacement noise were visible with either imaging condition. A histogram of the noise intensity data, for both imaging condition, indicates that the u and v displacement noise fields have a Gaussian intensity distribution with standard deviations presented in Table 1. It can be seen from Table 1 and Fig. 4 data bars that the integrated imaging conditions produced a smaller standard deviation in the intensity of the noise distributions. By integrating eight images using the same frame time, the standard deviation of the random noise in both the u and v displacement measurements decreased by 25–50%, and therefore integrated scans were used for the remainder of this study. Fourier transform of the data indicates that the horizontal (u) and vertical (v) displacement noise are also spatially random, with no linear image distortions visible in Fig. 4(b). The Fourier transform of the calculated strain fields indicates that the strain noise is not completely spatially random, but has a preferred orientation with respect to the straining direction. The noise is elliptical with the long axis perpendicular to the direction of the strain calculated. Note that for all images the loading direction is along the horizontal axis.

Following the room temperature measurements, a similar experiment was performed at 700°C , the sample was pre-loaded to a stress well below the proportional limit (337 MPa) and pairs of integrated images were acquired. Since the pair of images was acquired at the same stress level, the mean strain value should be zero. The horizontal and vertical displacement fields show similar characteristics to the room temperature measurements, having a Gaussian intensity distribution and a random spatial distribution, with standard deviation in the intensity presented in Table 1. The standard deviation (noise) in the displacement data at 700°C is larger than the data collected at room temperature, as shown in Table 1. Fourier transforms of the strain data indicate that the spatial distributions of the strains are not completely random. There is a slight, preferred orientation of the maxima and minima of the data. Instead of being circular in nature, the extrema are slightly elliptical with the major axis of the ellipse aligned perpendicular to the strain measurement direction: vertical

for e_{xx} , forty five degrees from horizontal for e_{xy} , and vertical for e_{yy} as seen in Fig. 5. This is consistent with the strain data calculated at room temperature, and indicates that the method of calculating strain causes some preferential alignment of the noise measurements.

Preliminary elevated temperature data

Bulk stress–strain data was calculated from the crosshead displacement measurements and is presented in Fig. 6, it can be seen that at the first load drop at which images were acquired the sample had experienced $1.45\pm 0.02\%$ strain. When the elastic portion of the strain below the DIC preload stress is subtracted from this value, it indicates that the average strain measured by DIC measurements would be $1.28\pm 0.02\%$.

Figure 7(b) shows the results of digital image correlation (DIC) analysis between the image taken at the preload stress (337 MPa) and an image taken after a 35 min hold at 1100 MPa. The average tensile strain from the DIC measurements was $1.48\pm 0.07\%$, which is in good agreement with the bulk data calculated from crosshead displacement, but may indicate that a larger area might be needed for better correlation. The maps in Fig. 7(b–d), along with the inverse pole figure map in Fig. 7(a), provide insight into the propensity for strain localization/inhomogeneity at elevated temperature. The magnitude of the high and low e_{xx} and e_{yy} strain measurements shown respectively in Fig. 7(b) and (d) are far greater than the standard deviation of the random noise calculated for these imaging conditions, as discussed above. Regions of high e_{xx} strain are often associated with grain boundaries, as shown in Fig. 7(b). These regions often correlate with cracks that form after even larger deformations, as discussed below. Regions of highly negative vertical strain, e_{yy} , routinely correlate to regions near those containing highly positive horizontal strain, e_{xx} , which is consistent with the need to maintain constant volume during plastic deformation. The e_{xy} data [Fig. 7(c)] indicates that regions of highly localized shear, either positive or negative, tend to correlate with grain boundaries in this sample. In general, strain inhomogeneity appears on a scale similar to the grain size of the material, which is consistent with the anisotropic deformation response of superalloys as a function of crystal orientation [17].

A magnified region of the deformed sample (from the top left corner of the microstructure presented in Fig. 7) is shown in Fig. 8. Several small cracks have been identified with arrows in Fig. 8(a). Several of these cracks and slip steps correlate with high angle grain boundary locations, which are superimposed from the EBSD map presented in Fig. 8(b). The high angle grain boundary at the upper right hand corner of this region has cracked. Correlating with

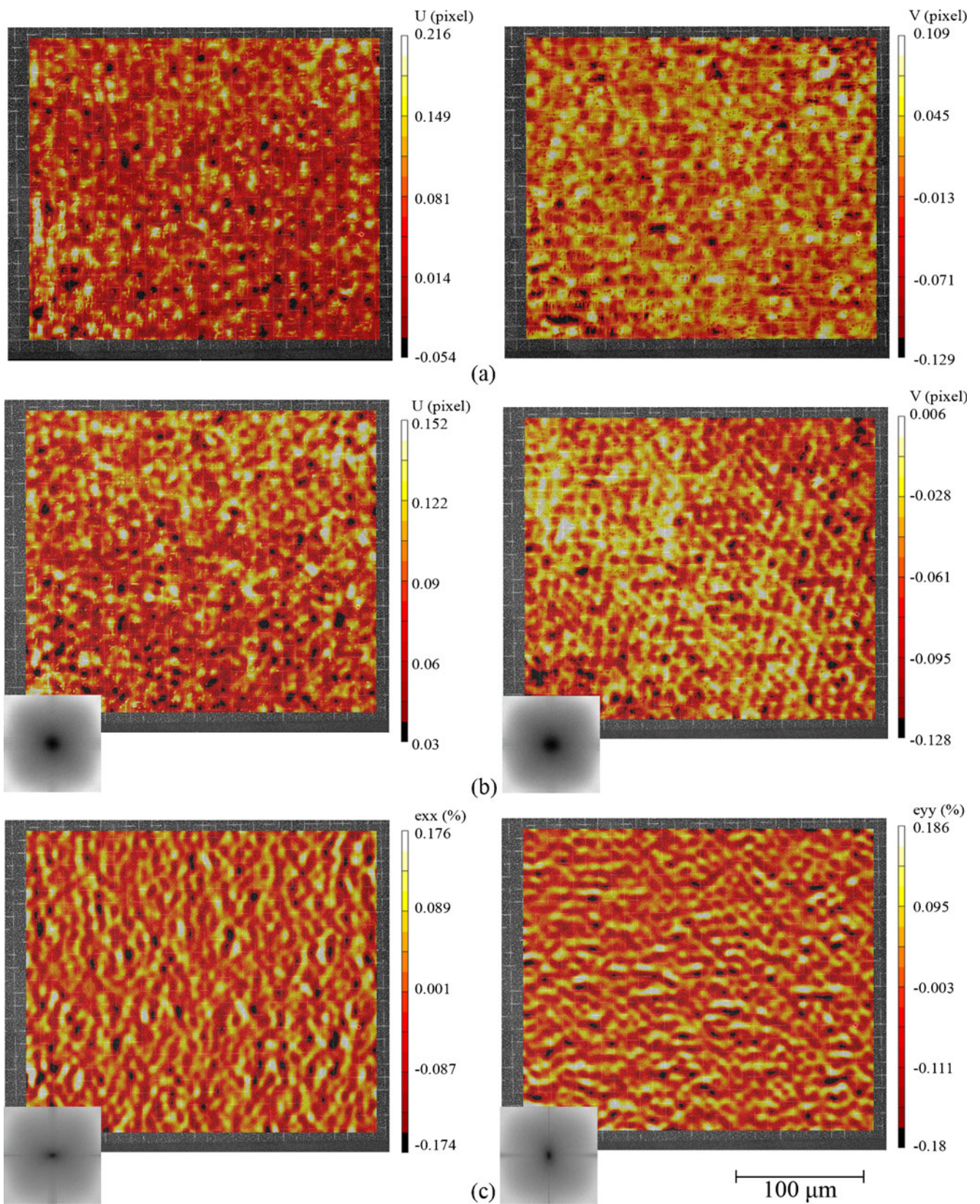


Fig. 4 horizontal (U) and vertical (V) displacement fields of a sample imaged at room temperature at 1000 \times magnification for (a) 8 μs dwell time with one scan and (b) 1 μs dwell time with eight integrated scans. The e_{xx} e_{yy} fields for 1 μs dwell (c) show a slightly nonrandom distribution

Fig. 8(c), which displays the strain localizations measured by the DIC software, indicates that the crack in this grain boundary is due to a localization of tensile strain, ϵ_{xx} . There is also large principle strain in the grain near the center of the field of view in Fig. 8(c), it can be seen that this deformation is associated with the twins in the grain. Large shear strains are also observed in the region presented in Fig. 8(b). The Schmid factors for $\langle 110 \rangle \{111\}$ and $\langle 112 \rangle \{111\}$ slip systems are shown in Fig. 8(e) and (f), respectively. Operation of both of these slip systems have been previously reported [17, 18], and are expected to both be active when deformation occurs at this strain rate. It is interesting that the influence of the annealing twin boundary in the central grain is manifested in the shear strain pattern [Fig. 8(b)]. In general, there is not a clear correlation between Schmid factors and plastic strain localizations based on these initial experiments.

Discussion

The present study demonstrates the feasibility of conducting *in-situ* SEM deformation studies in temperature and strain rate regimes relevant to high temperature structural materials. The correlation between localized deformation and microstructural features was assessed by correlating EBSD analysis of grain shape and orientation with DIC deformation maps. Yet to be resolved technical issues related to the application of this technique are as follows: distortions in the EBSD data, and intensity and spatial resolution limitations of the DIC analysis due to both the speckle pattern and noise associated with elevated temperature testing. In this section we will discuss in detail these issues and how they can be mitigated in future work.

The major limitation for implementing the data collected into computational models is the EBSD spatial distortions. The current method relies on manual manipulation of the image maps created by EBSD software and does not provide an adequate method for

transforming the raw data into a useful form. A method to remove distortion in the raw data is needed before correlation of crystallographic orientation with DIC. This issue can be resolved through careful application of the following techniques. First, care should be taken when aligning the specimen in the SEM chamber to ensure the sample surface is first truly perpendicular to the electron column before tilting to precisely for EBSD analysis. Verification of the tilting angle can be done using the crystallographic relationships of a single crystal silicon sample placed on the sample surface [19]. Further, the scans should be conducted at sufficient magnification to eliminate distortion due to excessive beam shifting. Finally, the scans must be stitched together to provide a continuous data set for the entire region of interest, this can be done using an open source Matlab code such as the AnyStitch program [20].

Intensity resolution and spatial resolution are the two primary issues associated with resolving strain. Intensity resolution is primarily a function of imaging specifications [8]. The intensity resolution is limited by the ability of DIC to recognize the shift of a speckle by a pixel width, therefore the relative focus of each speckle is important. The FEI microscope used in this study performs image integration by creating a single image where the final pixel intensity is the average intensity at each pixel for the set of collected images. If the specimen drifts during image collection, the speckle edges blur substantially, leading to significant degradation of the image. Therefore, while the image integration technique can minimize signal noise, the blurring of the speckle edges often limits the ultimate resolution that can be practically achieved using DIC. One potential method for maximizing the signal-to-noise ratio while minimizing the effects of specimen drift is to employ a pattern matching algorithm to align the sequence of images, thus eliminating systematic and random drift effects prior to image integration.

Spatial resolution of the full-field data is dependent on the image subset step size used for analysis, smaller step sizes will yield higher spatial resolution. For a given speckle pattern and image resolution there is a minimum step size and in-turn maximum spatial resolution. Using a step size smaller than this minimum size will yield inadequate correlation as each subset will not contain a unique speckle distribution, and will therefore not contain the requisite random grayscale. Thus, for a given image resolution, a higher speckle density will allow for a smaller step size. For a given image resolution there exists a maximum speckle density above which Moiré fringes occurs. This Moiré effect obscures unique speckles and causes a breakdown in the ability to conduct DIC. If the

Table 1 List of standard deviations for the noise in the displacement and strain measurements for single and integrated images taken at room temperature and 700°C

| | Standard deviation | | | | |
|-----------------------|--------------------|-----------|---------------------|---------------------|---------------------|
| | u (pixel) | v (pixel) | ϵ_{xx} (%) | ϵ_{yy} (%) | ϵ_{xy} (%) |
| single scan 20°C | 0.053 | 0.044 | 0.142 | 0.121 | 0.086 |
| integrated scan 20°C | 0.028 | 0.030 | 0.073 | 0.075 | 0.054 |
| integrated scan 700°C | 0.046 | 0.069 | 0.079 | 0.157 | 0.080 |

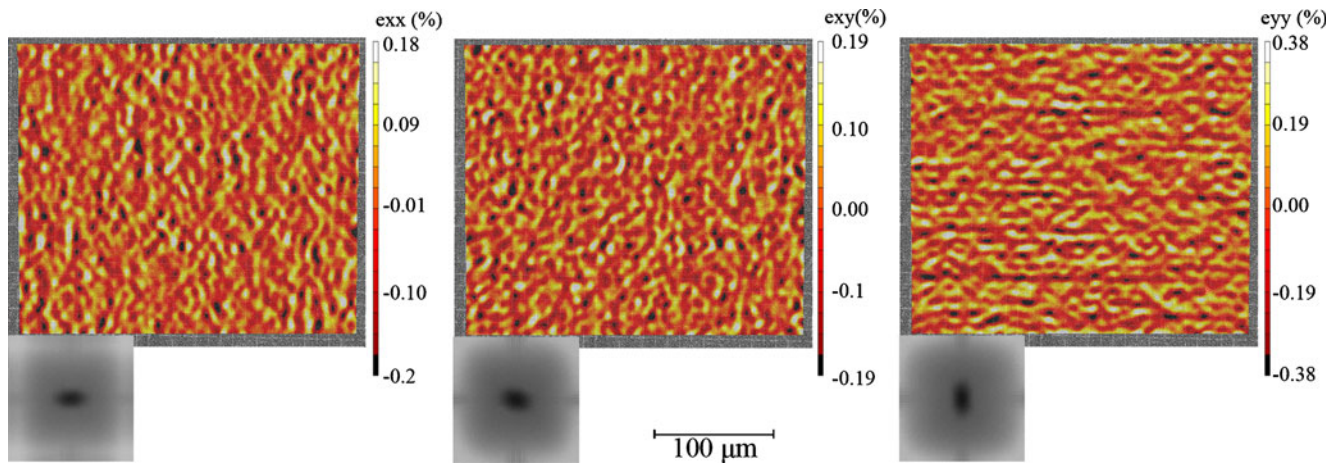


Fig. 5 Noise in the strain measurements as calculated from a pair of images (each with 1 μ s dwell, eight image integration) at 700°C and 337 MPa. The loading direction is horizontal

region of interest is analyzed using a single image, there is a trade-off between having the necessary spatial resolution to provide details on local displacement events and having the necessary field of view to observe multiple displacement events. A method for overcoming this paradox is to acquire overlapping images at high magnification with high speckle density to create an image montage. Such a montage will eliminate the paradox as long as image aberrations are minimized or corrected. Merging multiple image sets to acquire a larger field of view has been done

with optical DIC techniques and would be applicable to SEM based imaging techniques [5].

The shape of each speckle is also a factor for spatial resolution of DIC techniques. Previous work conducted by Biery et al. concluded that the orientation of square speckles effects vertical resolution of strain mapping technique as the rastering method of SEM image formation is continuous in the horizontal (or scan) direction and discrete in the vertical direction [6]. Biery observed that when the edges of square speckles are aligned with the beam scan direction the vertical resolution was limited by the number of scan lines. Rotating the square pixels an arbitrary amount so that speckle edges were not parallel to the scan direction increased the vertical resolution. Round speckles would eliminate the alignment issue associated with square speckles. Unfortunately, e-beam lithography patterning using a 25 nm step size on a square grid can not accommodate round speckles. The data collected in this study show a larger standard deviation in the e_{yy} data than the e_{xx} and e_{xy} data. The limited spatial resolution in the y-direction might be caused by speckle alignment. The e-beam lithography technique provides the valuable ability to tailor the speckle shape and density. New patterns are under development to gain a better understanding of how these variables can be tailored to optimize the DIC displacement calculations.

The technical issues addressed above are independent of testing temperature. The additional complexity of operating at elevated temperatures increases the standard deviation in the displacements by almost 2 times as compared with those calculated from room temperature images. This could indicate that this technique has limited application for measuring very small strains (e.g. for elastic modulus measurements), but should not limit the ability to use this technique to observe

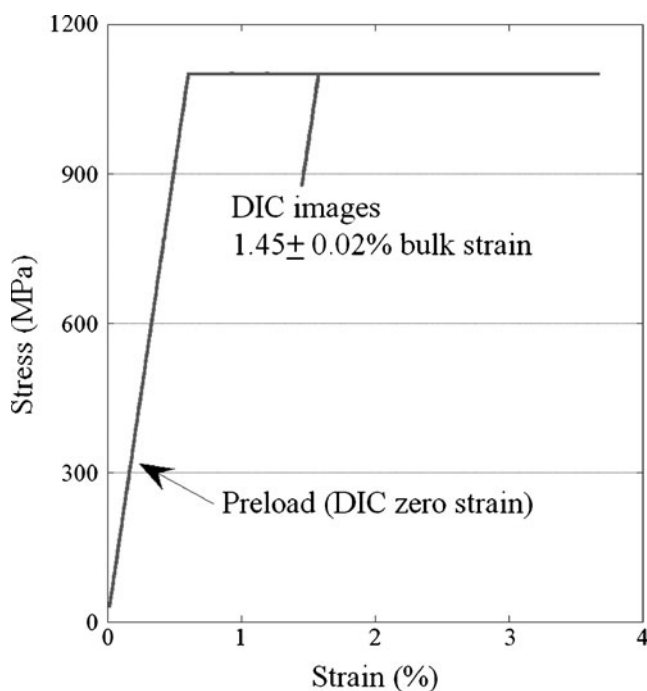


Fig. 6 Bulk stress–strain data showing the preload stress and stress drop during creep when images for DIC were acquired

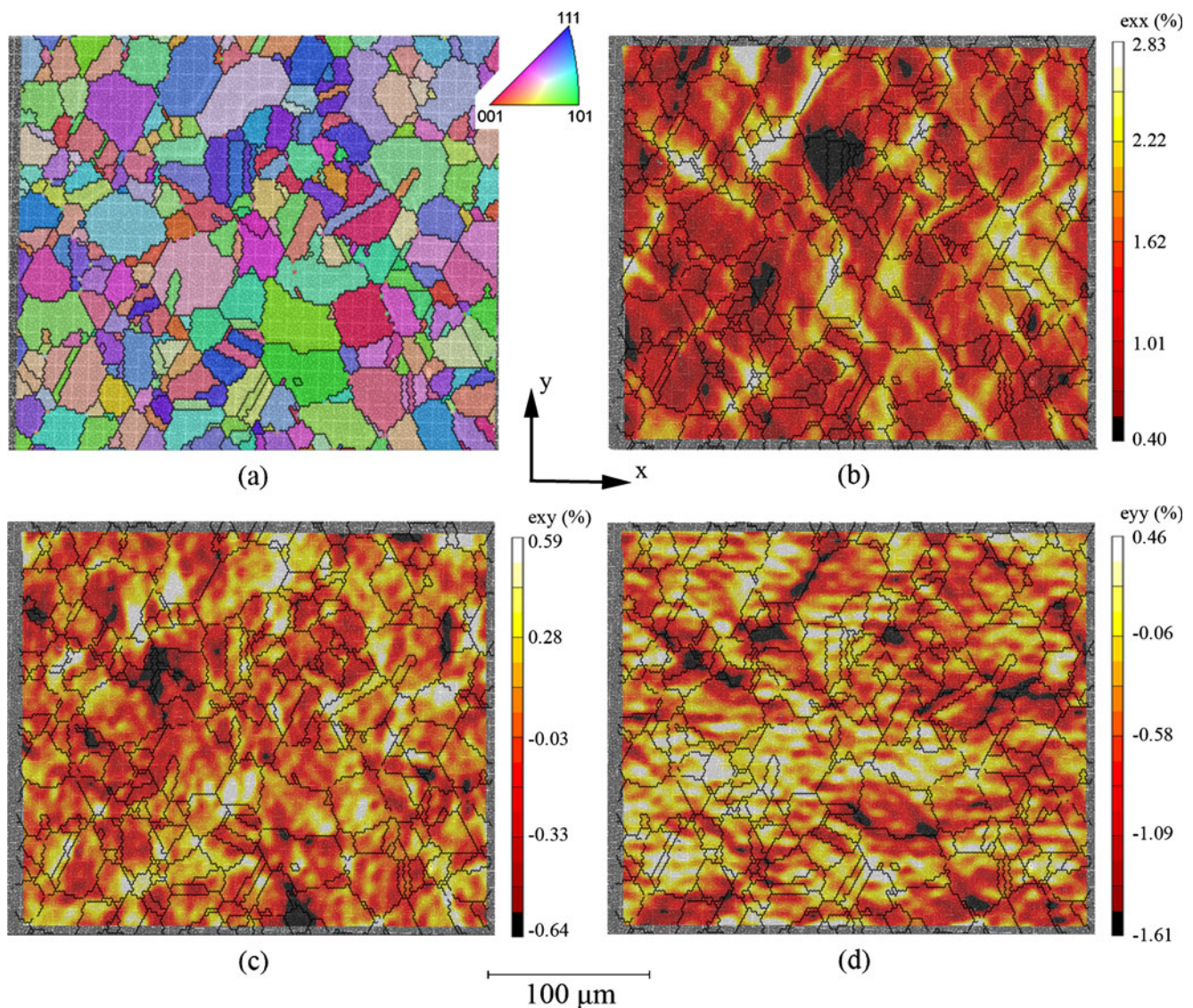


Fig. 7 (a) inverse pole figure map overlaying the speckle pattern and measurement of (b) tensile strain in the x-direction (c) shear strain and (d) tensile strain in the y-direction. The sample was loaded in creep along the horizontal direction in the image at a stress of 1100 MPa for 35 min

trends between regions of higher deformation and the microstructural features controlling them.

Inter-granular and intra-granular strain localizations were observable with this technique. At the particular stress examined, strains associated both with grain boundaries and grain interiors were detected. The surface strain measurements often correlated directly with surface slip steps and grain-scale cracks. Overall, there is not a clear correlation between local strain level and Schmid factor, which may indicate the importance of interacting grain neighborhoods in determining the local stress and strain development. There appears to be evidence of grain boundary sliding, the extent of which is still being analyzed, which is consistent with conclusions previously reported by Soula et al. [9]. This is particularly

interesting since these were observed in spite of the significantly larger stress levels, and in turn strain rates, imposed in the present study. Nevertheless, the present technique yields a direct correlation between 2-D localized deformation behavior and microstructure. As such, it is a powerful tool for examining how deformation behavior is controlled by a variety of characteristics, including: grain boundary character, 3-D boundary orientation relative to the stress axis (using subsequent FIB sectioning to reveal boundary orientations [21]) and second phase/impurity content (using FIB/TEM analysis [22]). The technique has the potential to provide valuable information that can be utilized to validate microstructure-sensitive, computational models of deformation that are being concurrently developed for these superalloys.

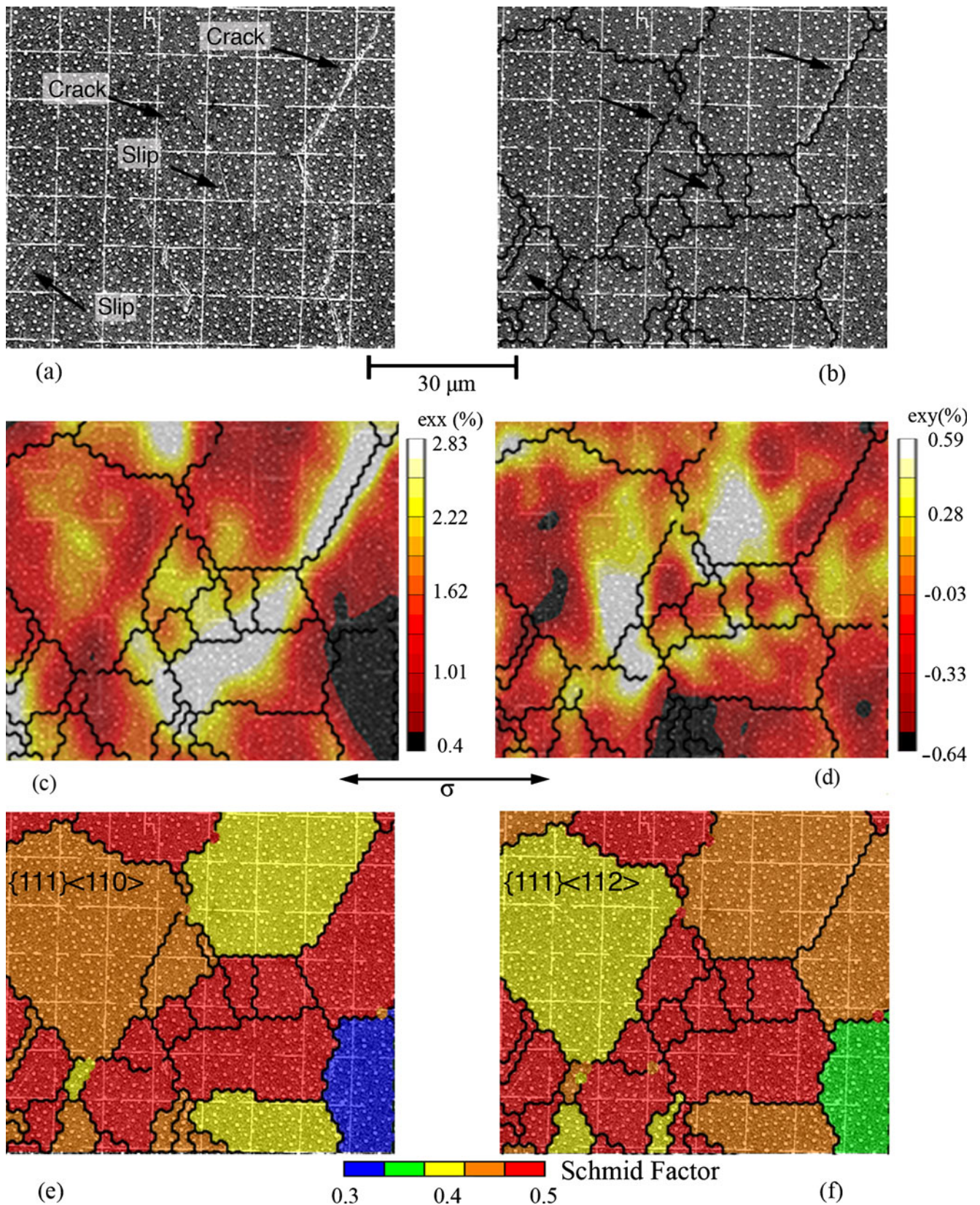


Fig. 8 (a) visible cracks and slip steps on the sample surface correlate with (b) high angle and twin boundaries. The principle (c) and shear (d) strain localizations measured by DIC also correlate with regions near grain boundaries with no clear correlation between strain localization and Schmid Factors for $\{111\}$ slip systems in (e) $\langle 110 \rangle$ or (f) $\langle 112 \rangle$ slip directions, high values of Schmid factor indicate easy deformation. Loading direction, σ , is horizontal

Conclusion

The present study has demonstrated a high temperature *in-situ* testing methodology that can produce high resolution full-field deformation maps which are ultimately applicable to physics-based crystal plasticity models. The novel patterning technique developed in this study provides adequate contrast in secondary electron imaging mode to facilitate digital image correlation. Further work is needed to address issues of spatial and intensity resolutions of the strain measurement if elastic modulus measurements are required, but these do not limit the ability of the present procedure to distinguish trends in deformation behavior as a function of microstructural features.

Preliminary strain data indicates that strain localization in Rene 104 occurs most often along grain boundaries. While it is not yet fully understood how orientation, misorientation, and grain size influence the strain distributions, it is conceivable that these factors may contribute to particular boundaries having high strain localizations while others do not.

The methodology described in the paper has demonstrated that adequate strain and spatial resolution can be obtained with an *in-situ* elevated temperature technique. The full field data collected can provide significant insight into both intra- and inter-granular deformation mechanisms in nickel-base superalloys at service-relevant temperatures and strain rates, and can ultimately be applied to other alloy systems and testing temperatures.

Acknowledgements This work is funded by the Air Force Research Laboratory (AFRL) STW-21 program FA9550-09-1-0014. The support received from the Materials & Manufacturing Directorate of the Air Force Research Laboratory has been instrumental for the development of the *in-situ* tensile frame. The authors would like to thank Aimee Price of the Ohio State University Institute for Materials Research and OSU Nanotech West Laboratory for her invaluable assistance with development on the lithography techniques for the speckle patterning.

References

1. Uchic MD, Dimiduk DA (2005) A methodology to investigate size scale effects in crystalline plasticity using uniaxial compression testing. *Mat Sci and Eng A* 400:268–278
2. Hemker KJ, Sharpe WN (2007) Microscale characterization of mechanical properties. *Annu Rev Mater Res* 37:93–126
3. Sutton MA et al (2009) Image correlation for shape, motion and deformation measurements. Springer, New York
4. Soula A et al (2009) Analysis of high-temperature creep deformation in a polycrystalline nickel-base superalloy. *Mat Sci Eng A* 510–11:301–306
5. Johnson DA (2009) Integrating experimentation, modeling, and visualization through full-field methods, SEM Annual Conference and Exposition, Albuquerque, NM, 1–4 June
6. Biery N et al (2003) A method for measuring microstructural-scale strains using a scanning electron microscope: applications to γ -titanium aluminides. *Met Mat Trans A* 34:2301–2312
7. Sutton MA et al (2007) Scanning electron microscopy for quantitative small and large deformation measurements—part II: experimental validation for magnifications from 200 to 10,000. *Exp Mech* 47:789–804
8. Sutton MA et al (2007) Scanning electron microscopy for quantitative small and large deformation measurements—part I: SEM imaging at magnifications from 200 to 10,000. *Exp Mech* 47:775–787
9. A. Soula, Y. Renollet, D. Boivin, J. L. Pouchou, D. Locq, P. Caron and Y. Brechet (2008) Grain boundary and intragranular deformations during high temperature creep of pm ni-based superalloys, in the proceeding from *Superalloys 2008*, TMS, Warrendale, PA, 387–93
10. W. Tu and T. M. Pollock (2008) Grain scale straining processes during high temperature compression of pm disk alloy, in the proceeding from *Superalloys 2008*, TMS, Warrendale, PA, 395–403
11. Reed RC (2006) The superalloys: fundamentals and applications. Cambridge University Press, United Kingdom
12. Scrivens WA et al (2007) Development of patterns for digital image correlation measurements at reduced length scales. *Exp Mech* 47:63–77
13. Langdon TG (2006) Grain boundary sliding revisited: developments in sliding over four decades. *J Mater Sci* 41:597–609
14. Zheng C (2008) Nanofabrication: principles, capabilities and limits. Springer Inc., New York
15. Fielden IM (2005) Investigation of microstructural evolution by real-time SEM of high-temperature specimens, Sheffield Hallam University
16. Seward GGE et al (2002) High-temperature electron backscatter diffraction and scanning electron microscopy imaging techniques: *in-situ* investigations of dynamic processes. *Scanning* 24:232–240
17. N. S. Tsuno, S., K. Takehi, C. M. F. Rae and R. C. Reed (2008) Tension/compression asymmetry in yield and creep strengths of ni-based superalloys, in the proceeding from *Superalloys 2008*, TMS, Warrendale, PA, 433–441
18. R. R. Unocic, L. Kavarik, C. Shen, P. M. Sarosi, Y. Wang, J. Li, S. Ghosh and M. J. Mills (2008) Deformation mechanisms in ni-base disk superalloys at higher temperatures, in the proceeding from *Superalloys 2008*, TMS, Warrendale, PA, 377–385
19. Baba-Kishi KZ (1998) Measurement of crystal parameters on backscatter kikuchi diffraction patterns. *Scanning* 20:117–127
20. Pilchak AL et al (2010) AnyStitch: a tool for combining electron backscatter diffraction data sets. *J of Microscopy*. (in press)
21. Li J et al (2009) Relative grain boundary area and energy distributions in nickel. *Acta Mat* 57:4304–4311
22. Mayer J et al (2007) TEM sample preparation and FIB-induced damage. *MRS Bull* 32:400–407